Journal of The Electrochemical Society, **155** (11) H852-H857 (2008)
0013-4651/2008/155(11)/H852/6/$23.00 © The Electrochemical Society

TaN_x Thin Films Deposited Through Various Flow Ratios of N_2/Ar for Copper Barrier Properties

Jem Kun Chen,[a,z] Chia-Hao Chan,[b] and Feng-Chih Chang[b]

[a]*Department of Polymer Engineering, National Taiwan University of Science and Technology, Taipei 106, Taiwan*
[b]*Institute of Applied Chemistry, National Chiao-Tung University, Hsinchu, Taiwan 30043*

To optimize copper diffusion barriers, TaN_x thin films for diffusion barriers were prepared by using radio frequency sputtering with various flow ratios of N_2/Ar as the reactive gas. The component transformed from Ta_2N to TaN as observed from deposition rates, and N/Ta ratios as N_2/Ar flow ratios from 0.075 to 0.3. Furthermore, the structural transformations from body-centered cubic through face-centered cubic to nanocrystalline for TaN_x thin film demonstrated under increase of N_2/Ar flow rate, induced three-step stages for formation of TaN_x films in the sputtering process. The thermal stabilities of the TaN_x thin film in Cu/TaN_x/n^+np^+ diodes suggest that increasing flow ratio of N_2/Ar from 0.075 to 0.3 enhanced the thermal stabilities from 450 to 550°C under leakage current conditions below 3 μA. The observation deduces that N_2/Ar flow ratios dominated predominantly properties of TaN_x films through crystal structure for barrier.
© 2008 The Electrochemical Society. [DOI: 10.1149/1.2969916] All rights reserved.

Manuscript submitted February 25, 2008; revised manuscript received July 22, 2008. Published September 5, 2008.

Copper metallization has been chosen for ultralarge scale integration due to its lower bulk resistivity (1.62 μΩ cm), better electromigration resistance, better stress-voiding resistance, and higher melting point (1084°C) than aluminum and aluminum alloys (Al–Si and Al–Si–Cu).[1,2] Copper has emerged as an alternative interconnect material to replace Al and Al alloys for deep submicrometer integrated circuits.[3] However, copper diffuses fast into SiO_2 or Si, and even reacts with Si at approximately 200°C.[4] To prevent the diffusion of Cu into SiO_2 and Si substrates of microelectronic devices, effective diffusion barriers are needed. The solubility of Ta in Cu and vice versa is very low in the solid state,[5] and silicide formation occurs at relatively high temperature only.[6] Thus, Ta-based layers are suited as diffusion barriers in Cu metallization.[7,8] Many diffusion barriers for copper metallization have been reported, such as transition metal barriers (Ta, W), transition metal nitrides (Ti–N, Ta–N, W–N),[9] and transition metal boride (TiB_2).[10] Especially, amorphous ternary diffusion barriers, such as (Ti, Ta)–Si–N,[11,12] have been attractive due to their good thermal stability with copper layers.

In thin Ta films, three modifications can be observed: the thermodynamically stable body-centered cubic (bcc) α-Ta,[13] the metastable tetragonal β-Ta,[14] and sometimes a face-centered cubic (fcc) phase.[15] Depending on the deposition parameters, a deposited Ta layer consists of either one or a mixture of the above-mentioned three phases.[15] Parameters determining this phase transformation are annealing temperature and time,[16,17] annealing ambience, substrate material, and film thickness.[18] Ta has a strong adhesion to Cu[19] but shows only a moderate adhesion to SiO_2.[20] Thus, the feasibility of growing the TaN thin films has been investigated extensively, particularly in terms of controlling the phase and microstructure of the TaN films to tightly control their barrier property.[21,22] Most of the investigations evaluated the property single-layered TaN barriers, indicating that cubic TaN barriers normally exhibit the highest chemical inertness and thermal stability among the remaining TaN barriers.[23-25] Due to the polycrystalline structure of Ta, grain boundary diffusion of Cu atoms becomes relevant at elevated temperatures.[26] One way to improve the thermal stability of Ta barrier layers is the addition of N during the deposition process. A lot of investigations were carried out to determine phase composition and microstructure of as-deposited TaN films depending on the N content.[27,28]

It is the aim of this publication to elucidate these properties for TaN_x barriers deposited onto SiO_2 and to compare their features with those of TaN_x films deposited with the mixture gas of N_2 and argon. Structural and compositional changes in the layer stacks were monitored with glancing-angle X-ray diffraction (XRD) measurements and transmission electron microscopy (TEM) investigations. X-ray photoelectron spectroscopy (XPS) was used for monitoring concentration changes of all atoms. Although there is a growing interest in graded Ta–TaN barrier layer stacks, less is known about microstructure and thermal stability in Cu/TaN_x/n^+np^+ diode systems. The Cu/TaN_x/n^+np^+ diodes were fabricated for electrical measurements in leakage current to analyze the thermal stabilities of the TaN_x diffusion barriers after rapid thermal anneal (RTA).[29]

Experimental

For the investigations of the graded Ta–TaN diffusion barriers, 4 in. n-type thermally oxidized silicon wafers with {111} planes and 525 ± 25 μm thickness was utilized as the substrate. Thermal oxidation was carried out at a temperature of 1000°C for 120 min in oxygen ambience to grow a 140 nm SiO_2 film. The wafers were cut into 1 × 1 cm squares, then a standard RCA[30] clean was performed prior to loading the wafers into the loadlock. The TaN_x thin films were deposited through radio frequency (rf) reactive sputtering by using N_2/Ar as the mixed reactive gases under 300 W of rf power. The base pressure in the physical vapor deposition chamber was 3×10^{-5} Pa and 150 mm of the target-to-substrate distance.

The N_2/Ar flow ratios were varied at 0.075, 0.100, 0.125, 0.150, 0.175, 0.200, 0.225, and 0.300 for nitrogen content in the sputter chamber under 4.0 Pa of sputtering pressure. The Ta target was sputtered for 30 min to clean the surface, the so-called presputter process. The samples were sputtered by the Ta target prepared by the presputter process, and all TaN_x thicknesses were around 150 nm. All samples were annealed under 10^{-4} Pa at 650°C for 3 h. Glancing-angle XRD measurements with an incidence angle of ω = 2° were done at room temperature in parallel beam geometry with Cu Kα radiation (λ = 15.418 nm) and thin-film equipment. The registered diffraction angle range was 2θ = 20–95° with a step size of Δ2θ = 0.05° and a measuring time of 40 s per step. TEM investigations were carried out with a JEOL 120EX microscope to identify the phase of the deposited films and crystal structure morphology. The deposition rates and roughness of the TaN_x thin films were observed by cross-sectional TEM and atomic force microscopy (AFM), respectively. XPS was utilized to analyze the N and Ta content in the TaN films and then the N/Ta ratio was estimated through these data.

The thermal failure property of the TaN_x thin film was tested through the leakage current by Cu/TaN_x/n^+np^+ diodes as shown in Fig. 1. The thicknesses of n^+, n, and p^+ layers in the n^+np^+ diode purchased from General Semiconductor were 20, 18, and 490 μm, respectively. The low-temperature oxide glass and medium-

[z] E-mail: jkchen@mail.ntust.edu.tw

Downloaded on 2014-04-25 to IP 140.113.38.11 address. Redistribution subject to ECS terms of use (see ecsdl.org/site/terms_use) unless CC License in place (see abstract).

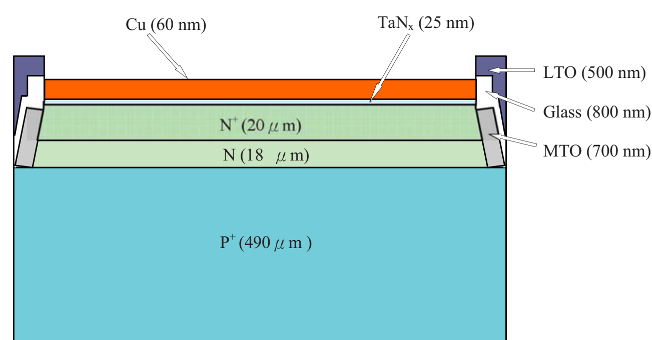

Figure 1. (Color online) The diode structure of a Cu/TaN_x (25 nm)/n^+np^+ sample for measurement of the leakage current at various temperatures.

temperature oxide around 500, 800, and 700 nm thick were utilized to isolate each diode, respectively. The 25 nm thick TaN_x films were deposited as barriers on the n^+np^+ surface with 0.075, 0.175, and 0.3 of N_2/Ar flow ratios in the sputtering chamber. Then a copper film with 60 nm thickness was deposited on the TaN_x films by rf reactive sputtering with argon at 3×10^{-5} Pa. The as-deposited $Cu/TaN_x/n^+np^+$ diodes were annealed in a rapid thermal vacuum annealer for 10 min under argon ambient at temperatures ranging from 450 to 650°C (±1°C accuracy) for RTA. The forward voltage was applied on the $Cu/TaN_x/n^+np^+$ diode, in which the negative voltage was connected with the copper electrode and the positive voltage was applied on the p^+ layer electrode. The current-voltage (*I-V*) curves were utilized to monitor the current passing through the diode from p^+ to the copper electrode, which was placed on the hotplate to increase the temperature from room temperature to 650°C as the forward voltage (−5 V) was applied on the diode. The leakage currents of the $Cu/TaN_x/n^+np^+$ diodes were measured by a Sony Tektronix 370A operated at an applied potential of −5 V at temperatures from 450 to 650°C for evaluation of the thermal properties.

Results and Discussion

Deposition rate and the composite of the TaN_x film.— Figure 2 shows the deposition rate of the TaN_x thin films and the N/Ta ratio estimated by XPS data in TaN_x films under various N_2/Ar flow ratios. The initial deposition rates of TaN_x thin films are approximated to 58 nm/min at N_2/Ar flow ratios from 0.075 to 0.125 and then decreased rapidly[31] at the flow ratios from 0.15 to 0.2, as shown in Fig. 2. Additionally, the N/Ta ratios increased from 0.3 to 0.57 with flow ratios from 0.075 to 0.125. This observation suggests that the formation composite of Ta and Ta_2N thin films induced the N/Ta ratio below 0.5. The increasing N/Ta ratio ascribes diffusion of the N element into the vacancy around the Ta structure from the mixed gases of N_2 and Ar. The rapidly decreasing deposition rate as the N_2/Ar flow ratio increased from 0.15 to 0.2 indicates that the component of the thin film transformed from Ta_2N to TaN, corresponding to the N/Ta ratio increase from 0.55 to 1.15. This suggests that the vacancies around the Ta atom were occupied gradually by N atoms, which induced the transformation from Ta_2N to TaN, corresponding to the decrease of the deposition rate. The TaN thin film was formed gradually as the N_2/Ar flow ratio rose above 0.175, as shown in Fig. 2. The deposition ratio decreased gradually to approximately 22 nm/min as flow ratios rose from 0.2 to 0.3 due to the formation of TaN thin film. The interstitials around the TaN structure are occupied by the N element, causing the N/Ta ratio to increase to above 1 as the N_2/Ar flow ratios increased from 0.2 to 0.3. This observation suggests that the mixture composite of the Ta and Ta_2N films with multiple phases were formed as the N_2/Ar flow ratio increased from 0.075 to 0.125, and the TaN films were formed as the N_2/Ar flow ratio rose from 0.175 to 0.2. The XPS spectra for Ta 4f

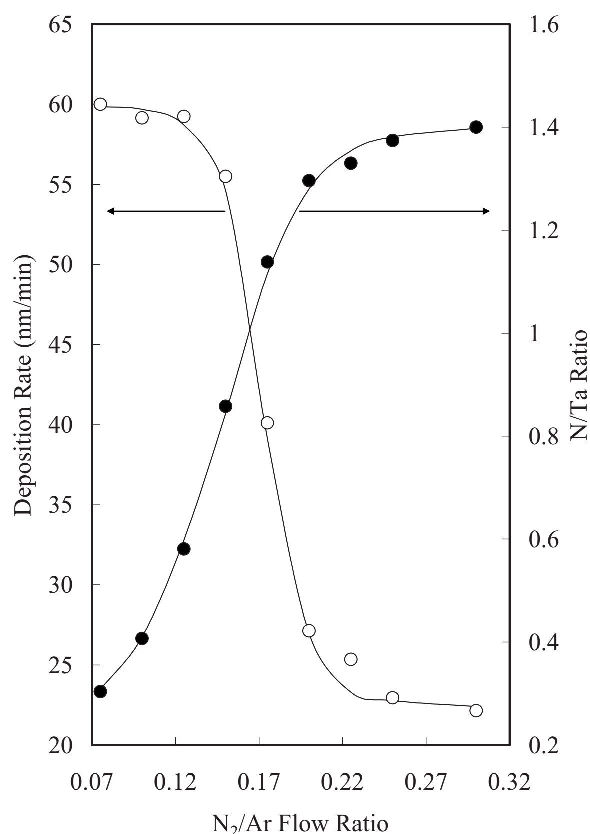

Figure 2. Deposition rates and N/Ta ratio in TaN_x thin films with respect to various N_2/Ar flow ratios after annealing at 600°C for 10 min.

in the TaN_x films deposited through various flow ratios of N_2/Ar are shown in Fig. 3. The binding energy of Ta $4f_{7/2}$ increased from 22.3 to 23.5 eV as the N_2/Ar flow ratio increased from 0.075 to 0.300. These Ta $4f_{7/2}$ peaks shifted to higher binding energies as the N_2/Ar flow ratios increased due to covalent shifting of Ta_2N to TaN in the thin films.[32]

Structure and morphology of the TaN_x film.— Figure 4 shows the XRD spectra obtained from the TaN_x thin films deposited with various flow ratios of N_2/Ar. The broad peak appears at angles of 38.7, which corresponds to the (101) reflections of hexagonal Ta_2N as N_2/Ar flow increases from 0.075 to 0.15. The broad peak is ascribed to the composite of Ta and Ta_2N in the bcc structure, which corresponds to a N/Ta ratio of 0.3–0.55. N/Ta ratio increased continuously as the flow ratio increased from 0.075 to 0.125, indicating that the thin films were composed mainly of Ta and Ta_2N. With the N_2/Ar flow ratio increasing, TaN film predominated in the films due to the obscure peaks for Ta_2N from the XRD spectra. The sharp peaks appear at diffraction angles of 35.2, 41.7, and 60.9, which correspond, respectively, to the (111), (200), and (220) reflections of TaN under fcc structure at a N_2/Ar flow ratio of 0.2. Therefore, the structures transformed from bcc (flow ratios of 0.075–0.125) to fcc (flow ratios of 0.175–0.200) polycrystalline structure. These peaks correspond to the disappearance of the fcc structure as the N_2/Ar flow ratio increased from 0.25 to 0.3, as deduced from the TaN structure transition from fcc to nanocrystalline.[32] This observation suggests that the interstitials around the TaN structure are occupied by N, which impeded the formation of fcc structure in the TaN films as N_2/Ar flow ratios rose from 0.2 to 0.3, inducing the nanocrystalline formation of TaN films.

The bright-field cross-sectional TEM images and diffraction patterns of TaN_x films for the various N_2/Ar flow ratios are shown in Fig. 5. Several spotted rings with larger radius and halo rings with

Downloaded on 2014-04-25 to IP 140.113.38.11 address. Redistribution subject to ECS terms of use (see ecsdl.org/site/terms_use) unless CC License in place (see abstract).

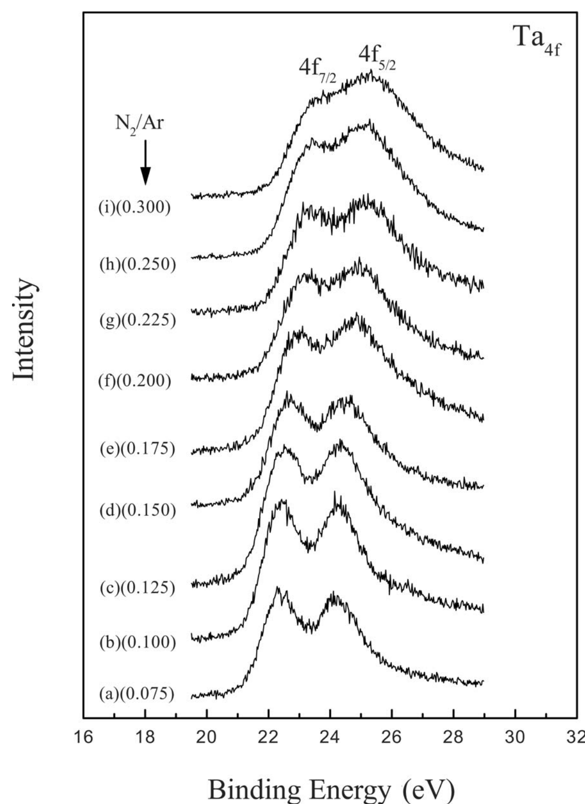

Figure 3. XPS spectra for Ta_{4f} in the TaN_x thin film deposited through a N_2/Ar flow ratio of (a) 0.075, (b) 0.1, (c) 0.125, (d) 0.15, (e) 0.175, (f) 0.2, (g) 0.225, (h) 0.25, and (i) 0.3 after annealing at 600°C for 10 min.

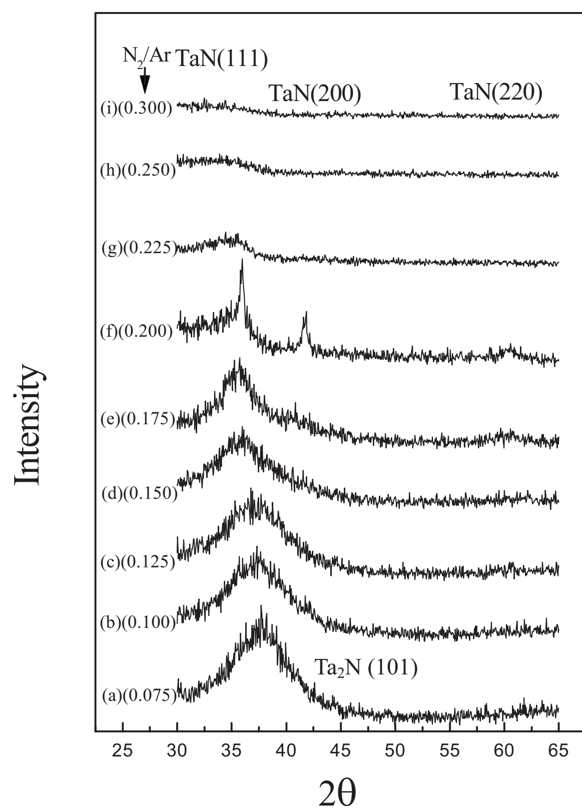

Figure 4. XRD spectra of the TaN_x thin films deposited through a N_2/Ar flow ratio of (a) 0.075, (b) 0.1, (c) 0.125, (d) 0.15, (e) 0.175, (f) 0.2, (g) 0.225, (h) 0.25, and (i) 0.3 after annealing at 600°C for 10 min.

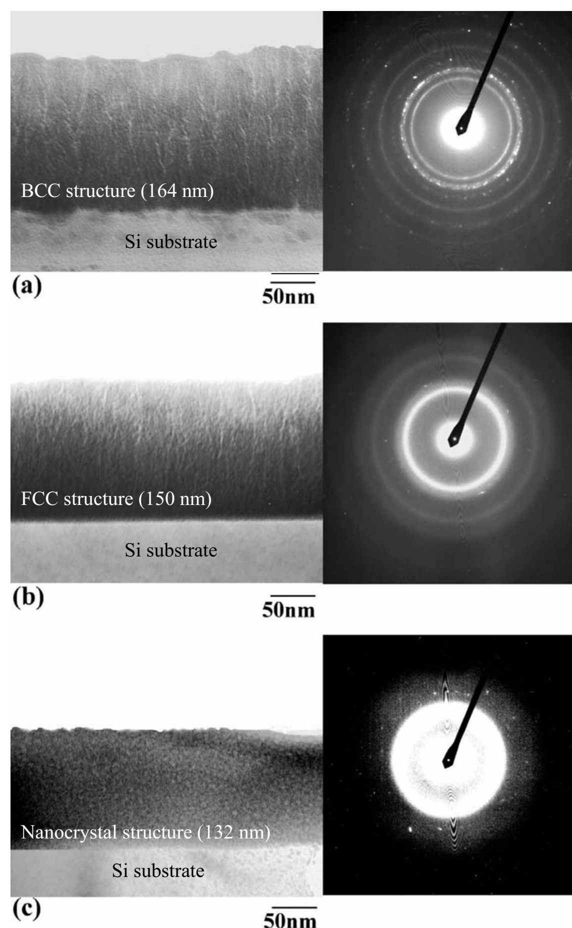

Figure 5. Bright-field cross-sectional TEM images and diffraction patterns of TaN_x thin films deposited through N_2/Ar flow ratios of (a) 0.075, (b) 0.175, and (c) 0.3 after annealing at 600°C for 10 min.

smaller radius (they contain only a few spots) can be seen, which correspond to interplanar spacings and interatomic distances as shown in Fig. 5a and b. Halo rings correspond to a little longer interatomic distance and spotted ones correspond to shorter ones than those of the polycrystalline structures. The TaN_x film demonstrates merely halo rings for TEM diffraction patterns due to the nanocrystalline structure, as shown in Fig. 5c. As the N_2/Ar flow ratio was 0.075, the Ta_2N thin film was formed into the bcc polycrystalline structure, verified by the ring pattern displayed in Fig. 5a, and the bright-field cross-sectional TEM images demonstrated the columnar-like structure. With increasing the N_2/Ar flow ratio to 0.175, the Ta_2N thin film transited to TaN thin film with fcc polycrystalline domain, verified by Fig. 5b and the bright-field cross-sectional TEM image, which indicates a preferred orientation of (111) corresponding to the XRD spectrum in Fig. 4e.[33] As the N_2/Ar flow ratio increased to 0.300, the TaN thin film with nanocrystalline structure demonstrates latticelike structure from the bright-field cross-sectional TEM image in Fig. 5c, corresponding to the XRD dispersive peaks in Fig. 4i. Bright-field plan-view TEM images of TaN_x thin films deposited through various N_2/Ar flow ratios are shown in Fig. 6. The bright-field plan-view TEM images indicated that the grain sizes decreased from 22.6 to 11.8 to 6.9 nm as flow ratios increased from 0.075 to 0.175 to 0.300, respectively. Additionally, the grain size and roughness estimated from Fig. 6 and AFM images shown in Fig. 7 are summarized in Table I. Figure 7 shows AFM results which demonstrate the surface morphology with roughness data, distinguishing the surface morphology mainly. The AFM images in Fig. 7 with (a) 0.075, (b) 0.175, and (c) 0.300 of

Downloaded on 2014-04-25 to IP 140.113.38.11 address. Redistribution subject to ECS terms of use (see ecsdl.org/site/terms_use) unless CC License in place (see abstract).

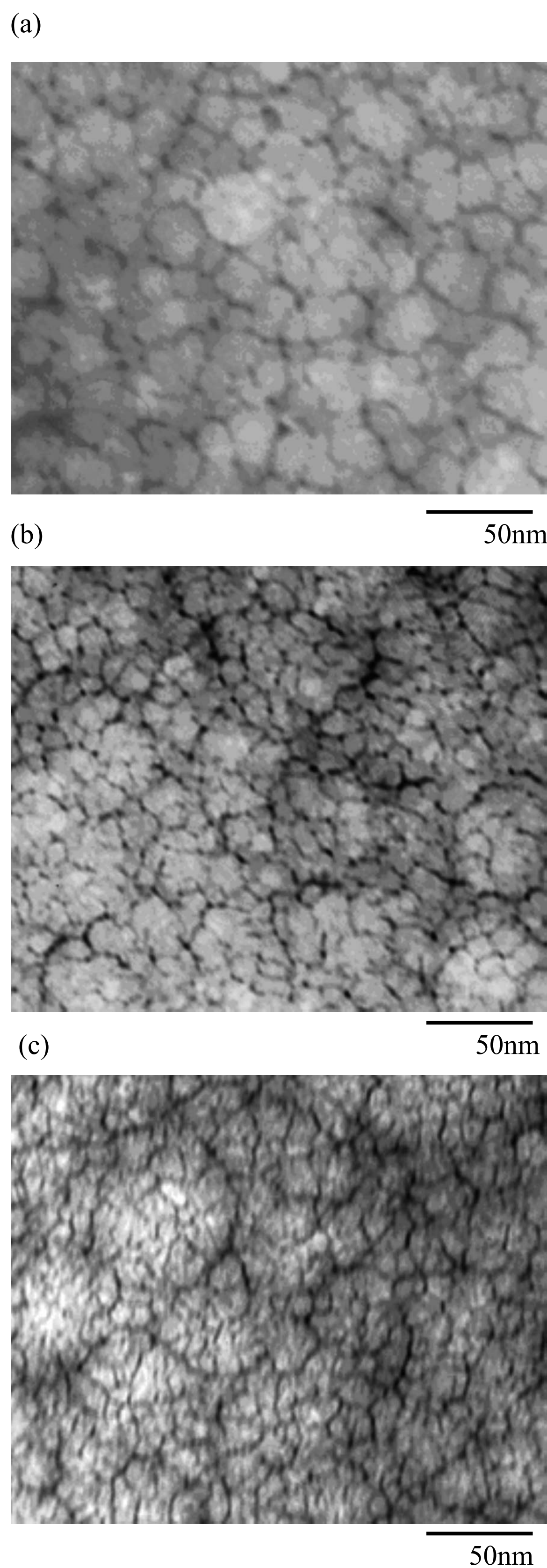

Figure 6. Bright-field plan-view TEM images of TaN_x thin films deposited through N_2/Ar flow ratios of (a) 0.075, (b) 0.175, and (c) 0.3 after annealing at 600°C for 10 min.

N_2/Ar flow ratios are similar images, showing the mixture structure under transformation from Ta_2N to TaN as the N_2/Ar flow ratio increases to about 0.175.

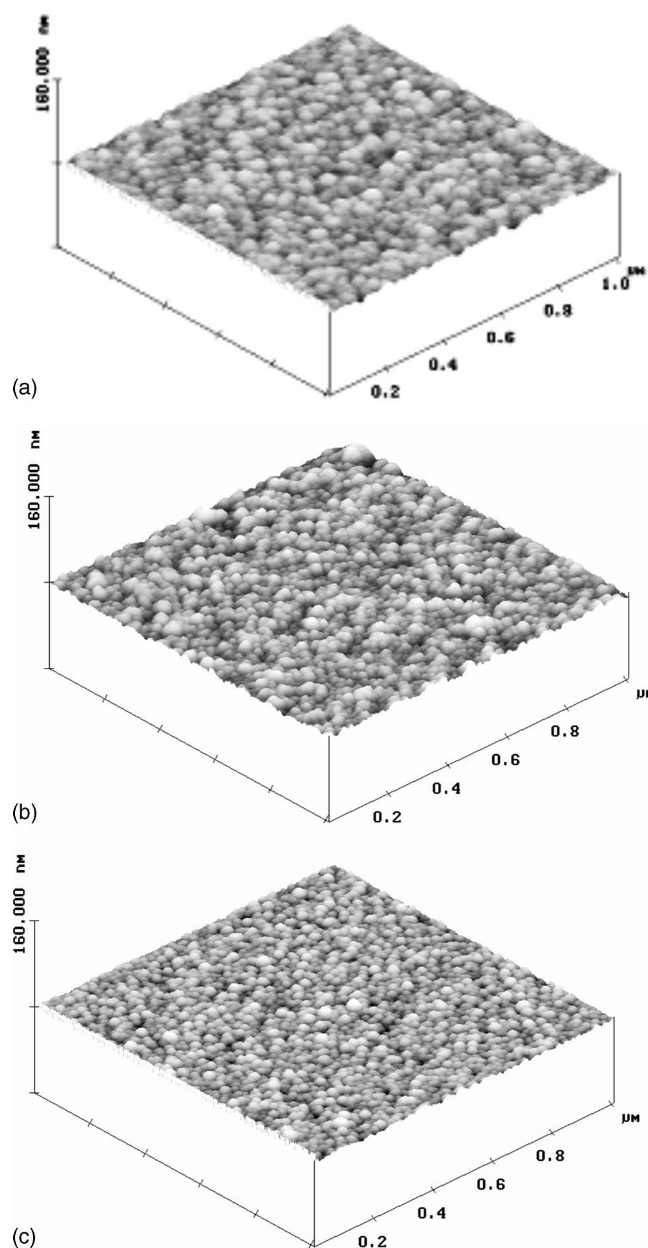

Figure 7. AFM images on TaN_x thin-film surfaces with (a) 0.075, (b) 0.175, and (c) 0.300 of N_2/Ar flow ratios after annealing at 600°C.

Grain densities calculated from these TEM images and resitivities of the TaN_x thin films were plotted as a function of N_2/Ar flow ratio in Fig. 8. Grain density approximated closed to a value as N_2/Ar flow ratio below 0.15 ascribes the bcc polycrystalline domain of Ta_2N films with 22.55 nm of grain size. As the N_2/Ar flow ratio rose above 0.175, the grain density increased rapidly due to the formation of fcc polycrystalline and nanocrystalline domain. We de-

Table I. The grain size and roughness estimated from AFM images with the various flow ratios.

N_2/Ar reactive gas flow ratio	Grain size (nm)	Surface roughness (nm)
0.075	22.6	4.7
0.175	11.8	2.8
0.300	3.9	1.5

Downloaded on 2014-04-25 to IP 140.113.38.11 address. Redistribution subject to ECS terms of use (see ecsdl.org/site/terms_use) unless CC License in place (see abstract).

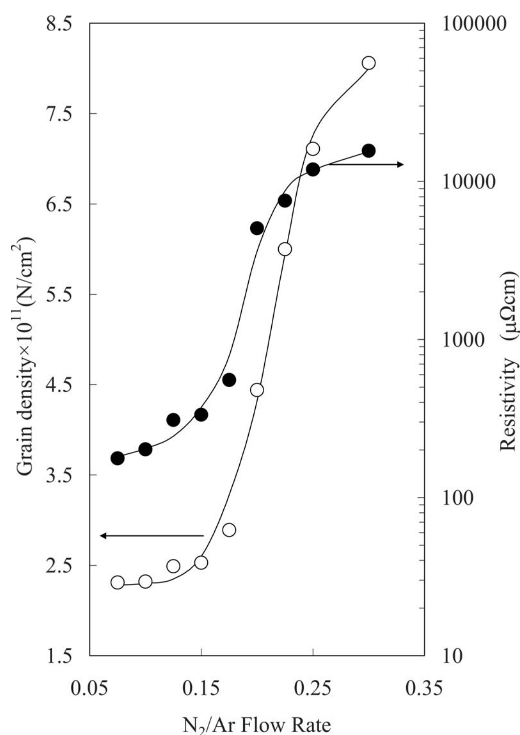

Figure 8. Grain densities and resistivities of TaN_x thin films deposited through the various N_2/Ar flow ratios after annealing at 600°C for 10 min.

fined the midpoint of the flow ratio from 0.175 to 0.225 as a critical ratio, which represented the transitional point from bcc to fcc polycrystalline domain. The resistivity increased gradually with the increase of N_2/Ar flow ratio from 0.075 to 0.15, and then rapidly increased as the N_2/Ar flow ratio increased above 0.175–0.25, the so-called critical ratio. The fcc polycrystalline formation of TaN films caused the rapid increase of resistivity as the N_2/Ar flow ratios rose above the critical ratio. This observation suggests that the resistivity of the TaN_x film corresponded to the grain density and the structure of the thin film. Increasing N content around the Ta atom varied the structure and the component of TaN_x film, inducing the increase of grain density. Therefore, the resistivity of TaN_x increased upon increase of N content, corresponding to the crystal structure. The TaN_x film resistivity of the crystal structure was concluded to be the following: bcc-Ta_2N < fcc-TaN < nanocrystal-TaN.

Thermal property for leakage current.— The leakage current for thermal treatment was measured under −5 V of forward voltage for Cu/$TaN_{1.13}$ (25 nm)/n^+np^+ diode at room temperature, 500°C, 550°C, and 600°C, respectively, to analyze the thermal stability as shown in Fig. 9. At room temperature, the electron was obstructed by TaN_x film, causing the leakage current to be −0.5 μA as −5 V of the forward voltage was applied on the diode. With a temperature increase to 500°C, the leakage current increased slightly to −1.5 μA at −5 V, as shown in Fig. 9b, suggesting that the copper atom was slightly diffused through barrier in the Cu/$TaN_{1.13}$ (25 nm)/n^+np^+ diode. The leakage current increased to −14 μA at −5 V, as shown in Fig. 9c, due to the diffusion of Cu through the TaN_x barrier layer into the n^+np^+ diode as temperature closed to 550°C. The leakage current increased to −1140 μA at the applied voltage, referring to the collapse of the TaN_x barrier layer as temperature approached 600°C, as shown in Fig. 9d. The observation suggests that copper atoms diffused slightly into the barrier layer at around 500°C, which caused the leakage current increase. The thermal capability for the TaN_x diffusion barrier was defined as the highest thermal stability under leakage current less than 3 μA with increasing temperature.[23] Table II summarizes the highest thermal stability temperatures of Cu/TaN_x/n^+np^+ samples ($x = 0.31$, 1.13, and 1.42) under 0.075, 0.175, and 0.300 of N_2/Ar flow ratio. The highest thermal stability for the TaN_x diffusion barriers increased with the N/Ta ratio due to the increasing electron charge cloud density from the N element, which resisted the copper diffusion through TaN_x film through repulsive force.[31] Thus, the TaN_x film demonstrated the optimum thermal property as the x value closed to 1.42.

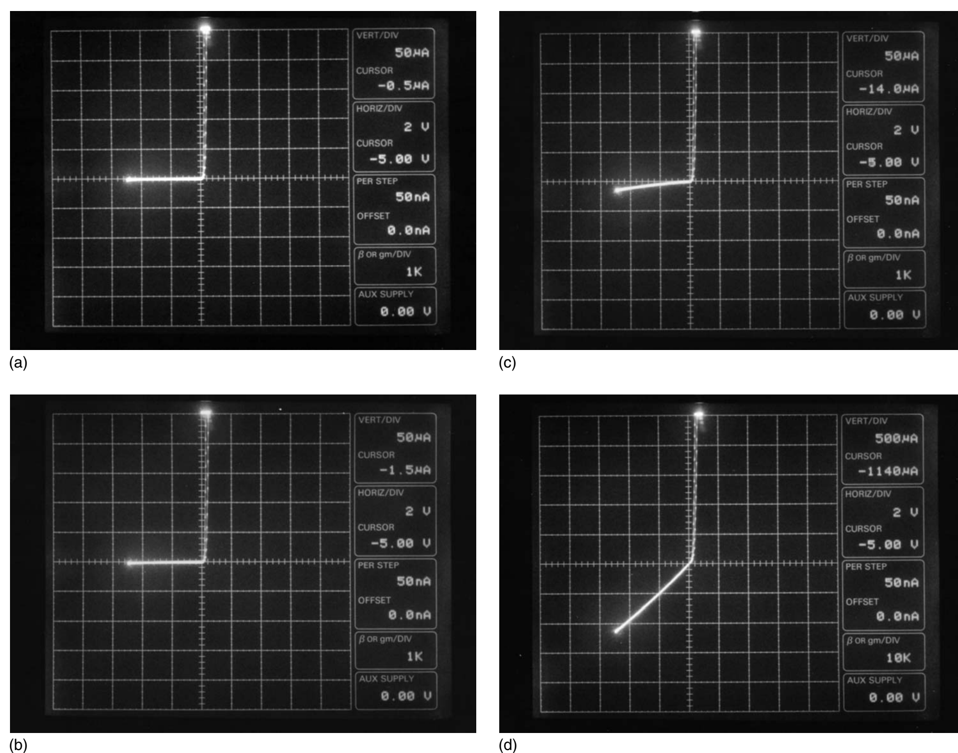

Figure 9. *I-V* curves as the forward voltage applied on the Cu/$TaN_{1.13}$ (25 nm)/n^+np^+ diode to measure the current at (a) room temperature, (b) 500°C, (c) 550°C, and (d) 600°C.

Downloaded on 2014-04-25 to IP 140.113.38.11 address. Redistribution subject to ECS terms of use (see ecsdl.org/site/terms_use) unless CC License in place (see abstract).

Table II. Highest thermal stability temperatures of Cu/TaN$_x$/n$^+$np$^+$ samples.

N_2/Ar reactive gas flow ratio	Cu/TaN$_x$(25 nm)/n$^+$np$^+$	The highest thermal stable temperature[a] (°C)
0.075	Cu/TaN$_{0.31}$(25 nm)/n$^+$np$^+$	450
0.175	Cu/TaN$_{1.13}$(25 nm)/n$^+$np$^+$	500
0.300	Cu/TaN$_{1.42}$(25 nm)/n$^+$np$^+$	550

[a] The highest thermal stable temperature, defined as the leakage current, was smaller than 3 μA with the increase of temperature.

Conclusions

The TaN$_x$ thin films deposited through various flow ratios of N_2/Ar demonstrated structural transition from bcc through fcc to nanocrystalline, corresponding to deposition rate, N/Ta ratio, and grain density of TaN$_x$ films. The results suggest that the N_2/Ar mixed gases dominated the formation of TaN$_x$ films in various structures and composition. Furthermore, the TaN$_x$ films were mainly composed of Ta_2N and TaN films in various structures by increasing the N_2/Ar flow ratio from 0.075 to 0.3, observed by the deposition rate in three step stages. The thermal stabilities of TaN$_x$ films were dependent predominantly on their crystal structure and composite. Increasing N/Ta ratios enhanced the thermal stabilities for the Cu/TaN$_x$/n$^+$np$^+$ diode structure to approach the optimum thermal property for copper barriers.

Acknowledgment

We thank the National Science Council of the Republic of China for financially supporting this research.

National Taiwan University of Science and Technology assisted in meeting the publication costs of this article.

References

1. J. Li, T. E. Seidel, and J. W. Mayer, *MRS Bull.*, **19**, 15 (1994).
2. K. S. Gadre, T. L. Alford, and J. W. Mayer, *Appl. Phys. Lett.*, **79**, 3260 (2001).
3. S. P. Murarka, *Mater. Sci. Eng., R.*, **R19**, 87 (1997).
4. L. Stolt, A. Chrai, F. M. D'Heurle, O. M. Fryer, and J. M. E. Harper, *J. Vac. Sci. Technol. A*, **9**, 1501 (1991).
5. P. R. Subramanian and D. E. Laughlin, *Bull. Alloy Phase Diagrams*, **10**, 652 (1989).
6. L. Liu, Y. Wang, and H. Gong, *J. Appl. Phys.*, **90**, 416 (2001).
7. L. A. Clevenger, N. A. Bojarczuk, K. Holloway, J. M. E. Harper, C. Cabral, R. G. Schad, F. Cardone, and L. Stolt, *J. Appl. Phys.*, **73**, 300 (1993).
8. T. Laurila, K. Zeng, J. K. Kivilahti, J. Molarius, and I. Suni, *J. Appl. Phys.*, **88**, 3377 (2000).
9. S. Q. Wang, *MRS Bull.*, **19**, 30 (1994).
10. J. Pelleg and G. Sade, *J. Appl. Phys.*, **91**, 6099 (2002).
11. J.-T. No, J.-H. O., and C. Lee, *Mater. Chem. Phys.*, **63**, 44 (2000).
12. D. Fisher, T. Scherg, J. G. Bauer, H.-J. Schultz, and C. Wenzel, *Microelectron. Eng.*, **50**, 459 (2000).
13. M. H. Mueller, *Scr. Metall.*, **11**, 693 (1977).
14. A. Arakcheeva, G. Chapuis, and V. Grinevitch, *Acta Crystallogr., Sect. B: Struct. Sci.*, **58**, 1 (2002).
15. P. N. Baker, *Thin Solid Films*, **14**, 3 (1972).
16. L. A. Clevenger, A. Mutscheller, J. M. E. Harper, C. Cabral, Jr., and K. Barmak, *J. Appl. Phys.*, **72**, 4918 (1992).
17. M. H. Read and C. Altman, *Appl. Phys. Lett.*, **7**, 51 (1965).
18. R. Hoogeveen, M. Moske, H. Geisler, and K. Samwer, *Thin Solid Films*, **275**, 203 (1996).
19. L. Chen, B. Ekstrom, and J. Kelber, *Mater. Res. Soc. Symp. Proc.*, **564**, 287 (1999).
20. M. Lane, R. H. Dauskardt, N. Krishna, and I. Hashim, *J. Mater. Res.*, **15**, 203 (2000).
21. J. C. Lin, G. Chen, and C. Lee, *J. Electrochem. Soc.*, **146**, 1835 (1999).
22. Y. J. Lee, B. S. Suh, M. S. Kwon, and C. O. Park, *J. Appl. Phys.*, **85**, 1927 (1999).
23. K. Wakasugi, M. Tokunaga, T. Sumita, H. Kubota, M. Nagata, and Y. Honda, *Physica B*, **239**, 29 (1997).
24. Y. J. Zhang, P. X. Yan, Z. G. Wu, W. W. Zhang, G. A. Zhang, W. M. Liu, and Q. J. Xue, *Phys. Status Solidi A*, **202**, 95 (2005).
25. M. H. Tsai, S. C. Sun, C. E. Tsai, S. H. Chuang, and H. T. Chiu, *J. Appl. Phys.*, **79**, 6932 (1996).
26. D. Fischer, O. Meissner, B. Bendjus, J. Schreiber, M. Starvev, and C. Wenzel, *Surf. Interface Anal.*, **25**, 522 (1997).
27. M. Stavrev, D. Fischer, C. Wenzel, K. Drescher, and N. Mattern, *Thin Solid Films*, **307**, 79 (1997).
28. C.-S. Shin, Y.-W. Kim, D. Gall, J. E. Greene, and I. Petrov, *Thin Solid Films*, **402**, 172 (2002).
29. M. T. Wang, Y. C. Lin, and M. C. Chen, *J. Electrochem. Soc.*, **145**, 2538 (1998).
30. E. Kolawa, J. S. Chen, J. S. Raid, P. J. Pokela, and M. A. Nicolet, *J. Appl. Phys.*, **70**, 1369 (1991).
31. T. Okamoto, M. Shimizu, A. Ohsaki, Y. Mashiko, K. Tsukamoto, T. Mastsukawa, and S. Nagao, *J. Appl. Phys.*, **62**, 4465 (1987).
32. X. Sun, E. Kolawa, J. S. Chen, J. S. Reid, and M.-A. Nicolet, *Thin Solid Films*, **236**, 347 (1993).
33. M. Takeyama, A. Noya, T. Sase, and A. Ohta, *J. Vac. Sci. Technol. B*, **14**, 674 (1996).

Downloaded on 2014-04-25 to IP 140.113.38.11 address. Redistribution subject to ECS terms of use (see ecsdl.org/site/terms_use) unless CC License in place (see abstract).